Iğdır Üniversitesi Fen Bilimleri Enstitüsü Dergisi, 15(3), 831-844, 2025 Journal of the Institute of Science and Technology, 15(3), 831-844, 2025

**Electrical Electronic Engineering** 

ISSN: 2146-0574, eISSN: 2536-4618

DOI: 10.21597/jist.1573764

#### Research Article

Received: 25.10.2024 Accepted: 07.04.2025

**To Cite:** Kaya, O. & Koç Polat, H. (2025). Miniaturized Aperture-Coupled Patch Antenna Through Metasurface Inspired DGS. *Journal of the Institute of Science and Technology*, 15(3), 831-844.

### Miniaturized Aperture-Coupled Patch Antenna Using Metasurface Inspired DGS

Osman KAYA<sup>1</sup>, Hilal KOÇ POLAT<sup>2\*</sup>

### **Highlights:**

- CubeSAT,
- antenna miniaturization,
- metasurface

### **Keywords:**

- Aperture coupled feed patch antenna,
- DGS,
- unit cell

### **ABSTRACT:**

In this paper, we present a new design of a compact aperture-coupled patch antenna for CubeSat applications. By loading a metasurface inspired defected ground structure (DGS) onto the ground plane of the aperture-coupled patch antenna, we achieved a miniaturized antenna that has 4.88 dBi realized gain, 96% efficiency, and 236 MHz bandwidth operating at 5.1 GHz. In addition, a conventional aperture-coupled patch antenna at 5.1 GHz was designed and compared with the miniaturized antenna. While the space covered by the conventional antenna is 1890 mm², the space covered by the miniature antenna is 622 mm². This corresponds to a reduction of approximately 67%. As a result, while the value of the conventional antenna was 30% better in terms of gain, it was seen that the bandwidth and efficiency were higher in the miniaturized antenna.

This study was produced from Osman Kaya's Master's thesis.

Osman KAYA (Orcid ID: 0000-0001-9035-9428), Milli Savunma University, Turkish Military Academy, Department of Electronics and Communications Engineering, Ankara, Turkiye

<sup>&</sup>lt;sup>2</sup> Hilal KOÇ POLAT (Orcid ID: 0000-0003-2382-1736), Erzurum Technical University, Department of Electrical and Electronics Engineering, Erzurum, Türkiye

<sup>\*</sup>Corresponding Author: Hilal KOÇ POLAT, e-mail: hilal.koc@erzurum.edu.tr

## INTRODUCTION

CubeSATs, known as nanosatellites that have gained popularity recently are being considered as an alternative to conventional satellites due to their less time development, and low fabrication costs (Liu et al., 2022).

The most critical component of CubeSat system, the antennas, are used to send and receive data to the ground station. Ensuring CubeSat success depends on the performance of the antenna. The antennas to be designed must have wide bandwidth (BW), high gain, and high efficiency while overcoming the low size and mass constraints of the CubeSat (Liu et al., 2022). For this purpose, miniaturization research of antennas is being conducted. Early research into antenna miniaturization shows that the reduction in size of an antenna often results in lower efficiency and limited bandwidth in the performance of the existing antenna. Later on, much new research has been conducted to reduce the overall size of different antenna types while trying to preserve bandwidth (Benzaghta et al.,2022; Baş & Kızılay, 2022).

Miniaturization techniques are basically divided into topology-based and material-based techniques. These techniques generally involve changing the electrical and physical properties of an antenna (Fallahpour et al., 2017). In antennas that are miniaturized with the meander line, high gain may not be achieved due to the out-of-phase nature of currents in adjacent arms. The radiation efficiency decreases with the fractal structure techniques. Miniaturization with DGS, the problem of noise may be created, which leads to issues with electromagnetic compatibility (Tadesse et al., 2020). Antennas including metamaterials or metamaterial inspired antennas using the general ideas of metamaterials to modify the resonant characteristics of antennas are two strategies that have attracted too much attention to overcome the limitations of conventional miniaturization methods lately (Singh et al., 2024).

In a study conducted by Arıcan and Karahan in 2022, the defected ground structure method was applied to reduce the size and enhance the operating frequency bandwidth (Arıcan & Karahan, 2023). In another study, thanks to the metasurface inspired DGS, an antenna showing superior performance characteristics in terms of bandwidth, gain, and efficiency when compared with the monopole antennas available in literature has been achieved (Raghavendra et al., 2023). In the comparison study (Moussa et al., 2022) between the slot miniaturization technique and the metamaterial miniaturization technique for the same initial antenna, it has been observed that the performance of the metamaterial miniaturization technique is better (higher gain and bandwidth with a higher miniaturization rate).

When the antenna types designed for CubeSats were examined (Abulgasem et al., 2021), it was found that the most popular antenna type was patch antennas, according to their suitability for CubeSat missions and usage rate. For wireless communications technology, compact patch antennas provide good options. For effective data transfer and reception, these antennas can be integrated with a variety of devices. Patch antennas are also advantageous when metamaterial-based techniques and metamaterial inspired structures are considered as antenna miniaturization techniques. Patch antennas have two drawbacks despite their many advantages: low gain and narrow bandwidth (Ataş et al., 2020). In this study, a novel approach based on metasurface inspired ground structure is presented for miniaturization of aperture-coupled patch antennas. The aperture-coupled feed, which is generally preferred in applications requiring wide bandwidth, has been preferred due to the versatility and flexibility of its basic design structure (Pozar, 1996; Celik & Karaçuha, 2022). The proposed antenna was fabricated, and the S<sub>11</sub> parameters were measured. The size and performance of the proposed antenna are promising for CubeSAT applications.

## MATERIALS AND METHODS

## The Configuration of the Miniaturized Antenna

The proposed miniature antenna design operating at 5.1 GHz starts with an aperture-coupled microstrip patch antenna operating at 8.0 GHz (initial antenna). The general structure and detailed representation of the preferred aperture-coupled antenna in design are given in (Figure 1).

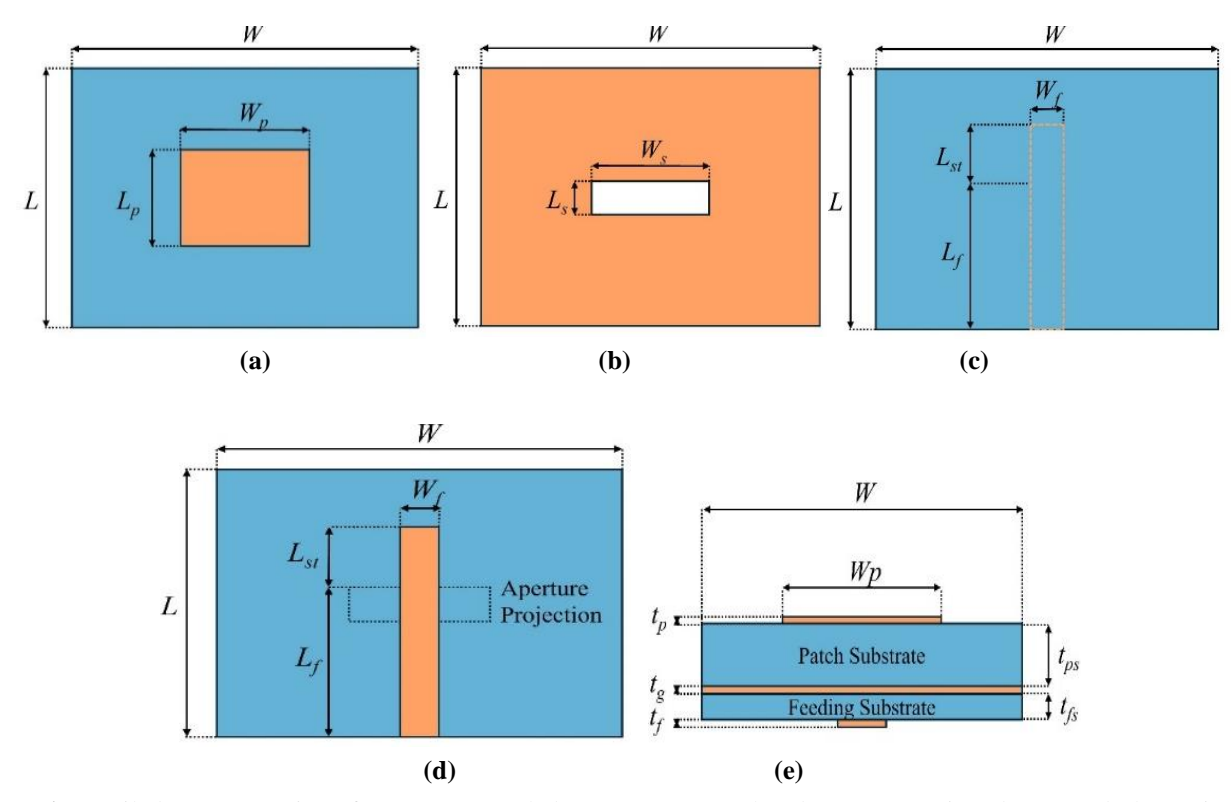


**Figure 1.** Detailed Representation of Aperture-Coupled Antenna, (a) Patch Substrate Top View (b) Ground Plane View (c) Feed Substrate Top View (d) Feed Substrate Bottom View (e) Antenna Side View

For antenna design, firstly, the patch dimensions were determined by the transmission line model used in the rectangular microstrip patch antenna design (Balanis, 2015). FR4 material ( $\epsilon$ r=4.3), which is commercially available and low cost, was preferred as patch substrate and feed substrate for the proposed antenna. In 2010, Civerolo have been determined the approximate substrate and slot dimensions of the aperture coupled antenna as follows. (Civerolo, 2010).

$$W = W_p + \lambda/2 \tag{1}$$

$$L = L_f x 2 \tag{2}$$

$$L_f = 0.528 \,\lambda$$
 (approximately  $\lambda/2$ )

$$L_{st} = 0.211 \,\lambda$$
 (approximately  $\lambda/4$ ) (4)

$$L_s = 0.0164 \,\lambda \tag{5}$$

$$W_{\rm S} = 0.1477\,\lambda\tag{6}$$

The initial antenna was designed using "Equations 1-6" and the most suitable antenna design was obtained by carrying out parametric studies on the dimensions. Analyses were performed using the CST Microwave Studio program. The geometry of the designed initial antenna is given in (Figure 2), and the physical parameter dimensions and expressions of the designed antenna geometry are presented in (Table 1).

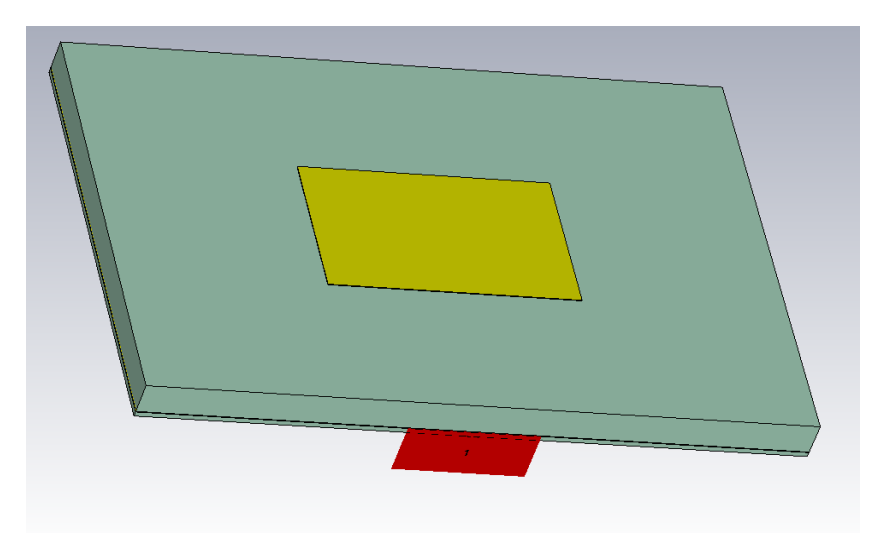


Figure 2. Initial Geometry Of Aperture-Coupled Antenna

**Table 1.** Design Parameters of the Initial Aperture Coupled Antenna

Name	Expression	Value (mm)		
L	Length of substrates	20.34		
W	Width of substrates	30.206		
$L_p$	Length of radiating patch	7.102		
$W_p$	Width of radiating patch	11.456		
$t_p$	Thickness of radiating patch	0.035		
$t_{ps}$	Thickness of patch substrate	1.6		
=	Thickness of ground plane	0.035		
$egin{aligned} t_g \ W_s \end{aligned}$	Width of coupling slot	0.374		
$L_{s}$	Length of coupling slot	5.291		
$t_{fs}$	Thickness of feed substrate	0.25		
$\hat{L}_f$	Length of feed	10.317		
$W_f$	Width of feed	0.5		
$t_f$	Thickness of feed	0.035		
$\dot{L}_{st}$	Length of the adjusting stub	2.725		

The reflection coefficients graph ( $S_{11}$  parameter) for the initial antenna is shown in (Figure 3) as a simulation result. When the graph is examined, it is seen that the initial antenna has a return loss value of -51.25 dB at 8.031 GHz and a bandwidth of 433 MHz.

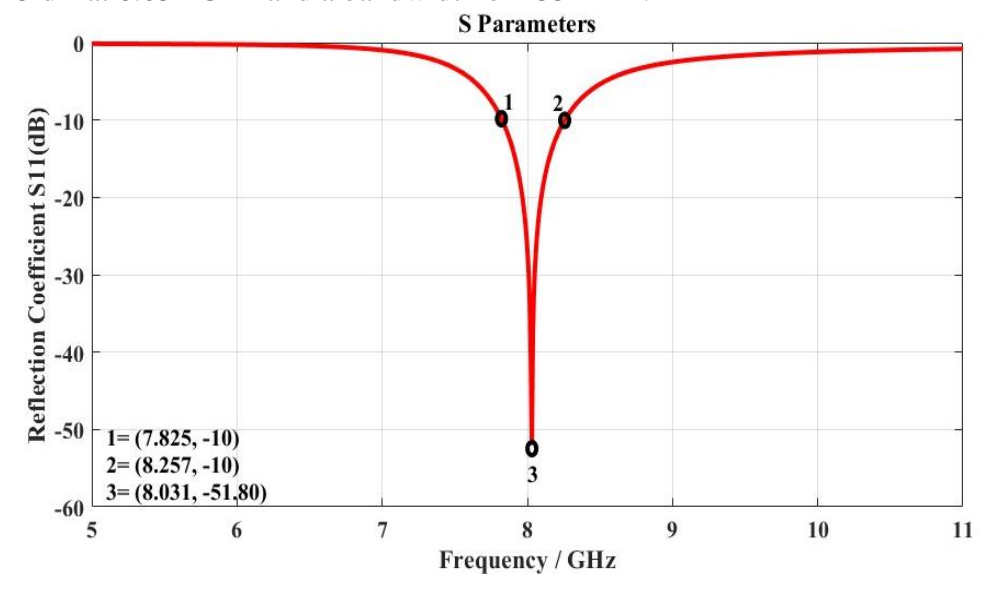


Figure 3. Reflection Coefficients of Initial Aperture-Coupled Antenna

In order to ensure that the initial antenna operating at 8.0 GHz can radiate at lower frequencies without changing its dimensions, square-shaped rings were inserted to the ground plane. In this way, it was aimed at reducing to lower frequencies, and the performance of the antenna at the relevant frequencies was examined. Step-by-step design shapes are shown in (Figure 4). The return loss graphs of these designs are presented in (Figure 5).

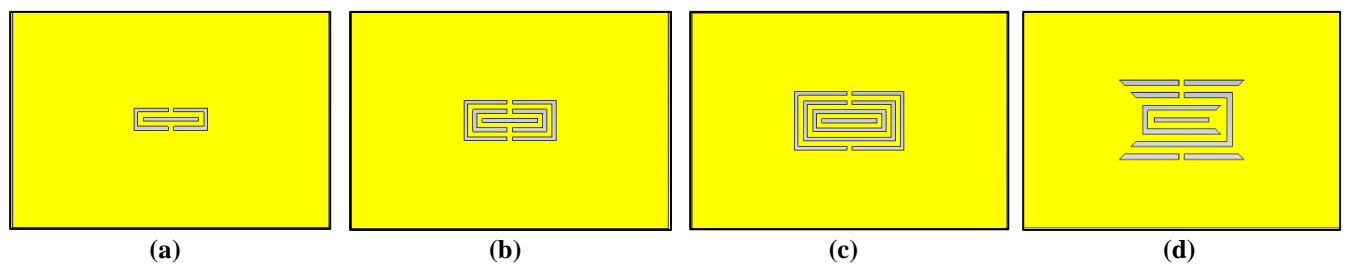


Figure 4. Metasurface Inspired DGS Antenna Designs (a) Design-1, (b) Design-2, (c) Design-3, (d) Design-4

The design was started by inserting a rectangular ring-shaped slot around the coupling aperture as depicted in (Figure 4a). Thus, it was seen that the operating frequency shifted slightly towards the lower frequency. Later, a second rectangular slot was inserted to the designed structure as depicted in (Figure 4b). Whether or not a slot is inserted to the parts of the microstrip feed on the ground plane changes the antenna performance considerably. Therefore, parametric studies were run in the simulation program to find the most suitable performance. As a result of the parametric studies, it is seen in (Figure 5) that the operating frequency for Design-2 has decreased to approximately 7.24 GHz. In the next stage, a third rectangular slot was inserted. With the parametric studies carried out, it was observed that the antenna radiated below 6.0 GHz. However, it is thought that the bandwidth is at a low level at the relevant frequency. Different topologies were tried on Design-3, and the final design (Design-4) in (Figure 4d) was obtained. The final antenna has a bandwidth of 0.236 MHz at 5.095 GHz and a 4.5% fractional bandwidth.

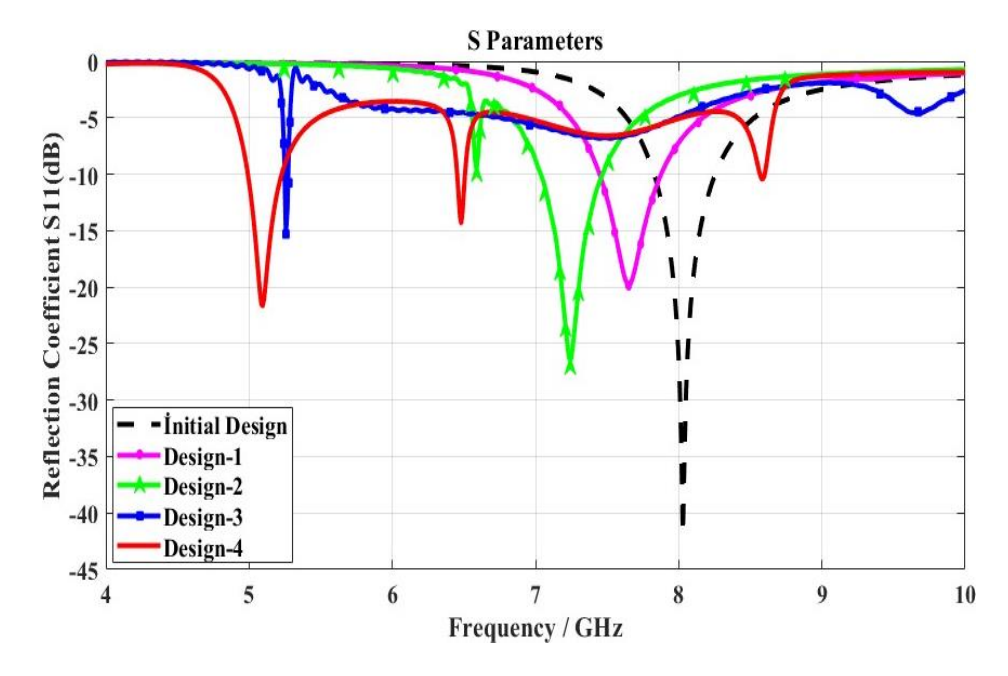


Figure 5. Reflection Coefficients of Metasurface Inspired DGS Designs

5.0

### **Coventional Antenna**

In this study, a miniaturized antenna operating at 5.1 GHz has been designed. In order to demonstrate the miniaturization extent of the antenna, a conventional aperture-coupled antenna has been designed at 5.1 GHz frequency. The physical dimensions of the antenna are given in (Table 2).

Name	Expression	Value (mm)	
L	Length of substrates	40.71	
W	Width of substrates	46.25	
$L_p$	Length of radiating patch	11.8	
$\dot{W_p}$	Width of radiating patch	17.6	
$t_p$	Thickness of radiating patch	0.035	
$t_{ps}$	Thickness of patch substrate	1.6	
$t_g$	Thickness of ground plane	0.035	
$\hat{W}_s$	Width of coupling slot	0.55	
$L_{\rm s}$	Length of coupling slot	7.0	
$t_{fs}$	Thickness of feed substrate	0.25	
$\hat{L}_f$	Length of feed	15.87	
$W_f$	Width of feed	0.5	
$t_f$	Thickness of feed	0.035	

 Table 2. Design Parameters of the Conventional Aperture Coupled Antenna

The reflection coefficients ( $S_{11}$ ) graph of the conventional antenna is shown in (Figure 6) as a simulation result. When the graph is examined, it is seen that the conventional antenna has a return loss value of -17.7 dB at 5.12 GHz and a bandwidth of 160 MHz.

Length of the adjusting stub

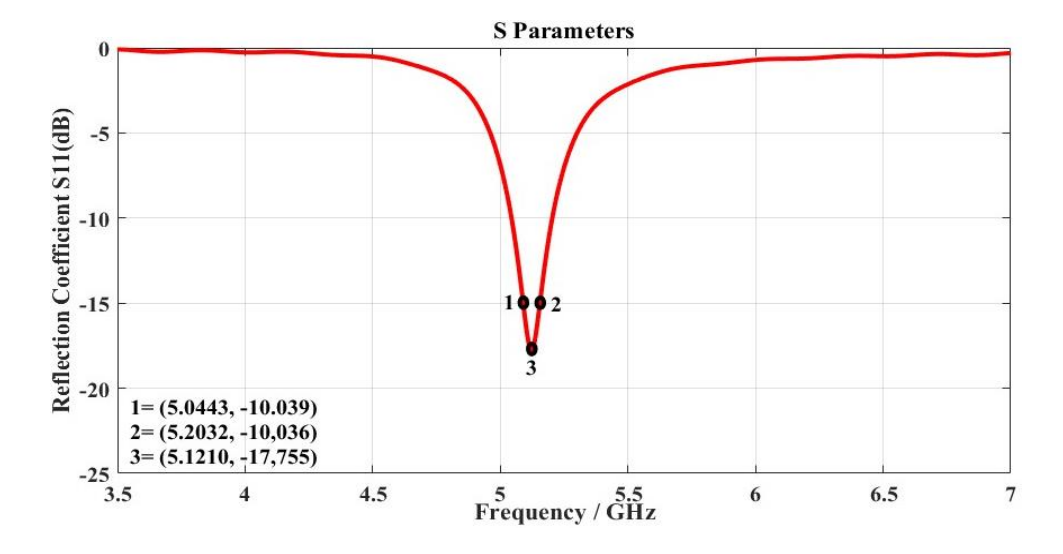


Figure 6. Reflection Coefficients of Conventional Aperture-Coupled Antenna

## Unit cell validation

Metamaterials are artificially produced materials that do not exist in nature and have unusual electrical properties (Ünal & Doğan, 2020). The classification of metamaterials is based on the basic parameter values such as  $\mu$ -positive and  $\epsilon$ -positive double positive (DPS),  $\epsilon$ -negative (ENG),  $\mu$ -negative (MNG), and double negative (DNG). Electromagnetic behavior in metasurfaces is illustrated through fundamental Maxwell equations "Equations 7. and 8." (Iqbal & Khan, 2022).

$$\nabla x \ \bar{E} = -j w \mu \ \bar{H} - \ \bar{M}_S \tag{7}$$

$$\nabla x \ \overline{H} = jw\varepsilon \ \overline{E} - J_{s} \tag{8}$$

 $\overline{E}$  and  $\overline{H}$  are respectively the electric field and magnetic field vectors,  $\overline{M}_s$  is the magnetic current density and  $\overline{J}_s$  is the electric current density. Considering plane waves, the  $\overline{E}$  and  $\overline{H}$  magnetic field vectors are given in "Equation 9." and "Equation 10.".

$$\bar{E} = \bar{E_0} e^{-j \ \bar{\beta}. \ \bar{a}} \tag{9}$$

$$\bar{H} = \bar{E_0} / \eta \, e^{-j \, \bar{\beta}. \, \bar{a}} \tag{10}$$

where  $\bar{\beta}$  is the wave propagation constant,  $\bar{a}$  is the decay constant, and  $\eta$  is the intrinsic impedance.

Information about the electromagnetic metasurface is obtained by substituting the expressions in "Equation 9." and "Equation 10." into "Equation 7." and "Equation 8." respectively. The response of the right-handed medium (where  $\epsilon$ ,  $\mu$  >0) for source-free regions where  $\overline{M}_s = \overline{J_s} = 0$  is presented in "Equation 11." and "Equation 12.". The case of left-handed medium (where  $\epsilon$ ,  $\mu$  <0) is presented in "Equation 13." and "Equation 14.".

$$\bar{\beta x} \ \bar{E} = +w\mu \ \bar{H}$$
 (11)

$$\overline{\beta}x \ \overline{H} = -w\varepsilon \ \overline{E} \tag{12}$$

$$\bar{\beta x} \ \bar{E} = -w|\mu| \ \bar{H} \tag{13}$$

$$\bar{\beta x} \ \bar{H} = +w|\varepsilon| \ \bar{E} \tag{14}$$

Validation of unit cell design, numerical extraction of parameters via Kramers-Kronig rule and Nicholson-Ross-Weir can be explained (Iqbal & Khan, 2022). In this study, the properties of the material have been extracted using CST. The final miniature antenna was designed as a unit cell consisting of three rectangular slots, 0.5 mm wide and 0.6 mm apart, centered on the coupling aperture in the ground layer. In order to calculate the  $\mu$  and  $\epsilon$  values in the unit cell verification, the  $S_{21}$  and  $S_{11}$  parameters need to be calculated. Therefore, as shown in (Figure 7), two separate ports were placed on the non-radiating edges of the antenna, and the results obtained from the CST microwave program Time Domain solution are presented in (Figure 8). When the graphs given in Figure 8 are examined, the designed initial antenna satisfies the positive  $\mu$  and positive  $\epsilon$  values at the resonance frequency (fr), the final miniature antenna satisfies the negative  $\mu$  and positive  $\epsilon$  values ( $\mu$  negative metasurface) at the resonance frequency.

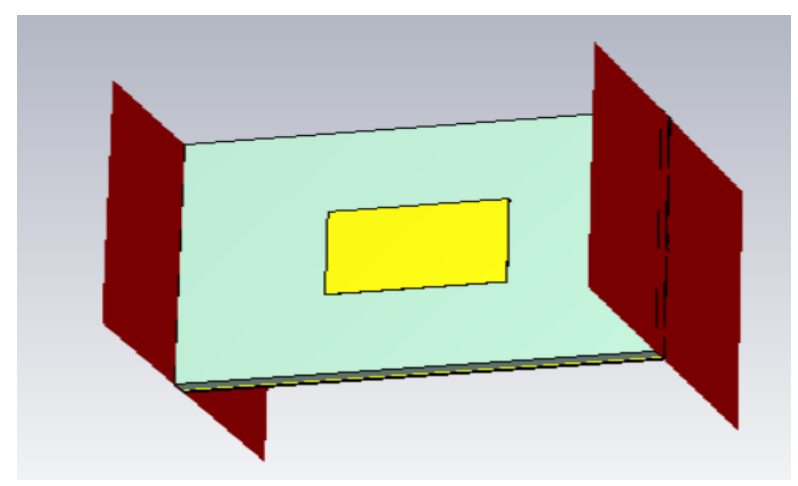


Figure 7. Two-Port Model of Antenna in CST for Unit Cell Analysis

The verification of the negative  $\mu$  and positive  $\epsilon$  values using the Nicolson Rose Weir (NRW) method is given by the following formulas:

$$X = \frac{S_{11}^2 - S_{21}^2 + 1}{2S_{11}} \tag{9}$$

"Equation 10." is used to calculate the reflection coefficient using the X value. The transmission coefficient T is given as in "Equation 11.".

$$\Gamma = X \pm \sqrt{X^2 + 1} \tag{10}$$

$$T = \frac{S_{11} + S_{21} - \Gamma}{1 - (S_{11} + S_{21})\Gamma} \tag{11}$$

$$\frac{1}{\Lambda^2} = -\left[\frac{1}{2\pi L}\ln(1/T)\right]^2 \tag{12}$$

The following is the permeability:

$$\mu_r = \frac{1+\Gamma}{\frac{1}{\Lambda}(1-\Gamma)\sqrt{1/\lambda_0^2 - 1/\lambda_c^2}} \tag{13}$$

The following is the permittivity:

$$\varepsilon_r = \frac{\lambda_0^2}{\mu_r} \left[ \frac{1}{\lambda_c^2} - \frac{1}{2\pi L} \ln(1/T) \right] \tag{14}$$

where L is the length of the sample and  $\lambda_0$  and  $\lambda_c$  are the free-space and cut-off wavelengths, respectively. Using the "Equations 13 and 14", the NRW method's computed values for  $\epsilon$  and  $\mu$  are, respectively, -4.01 and 110.08, confirming the models.

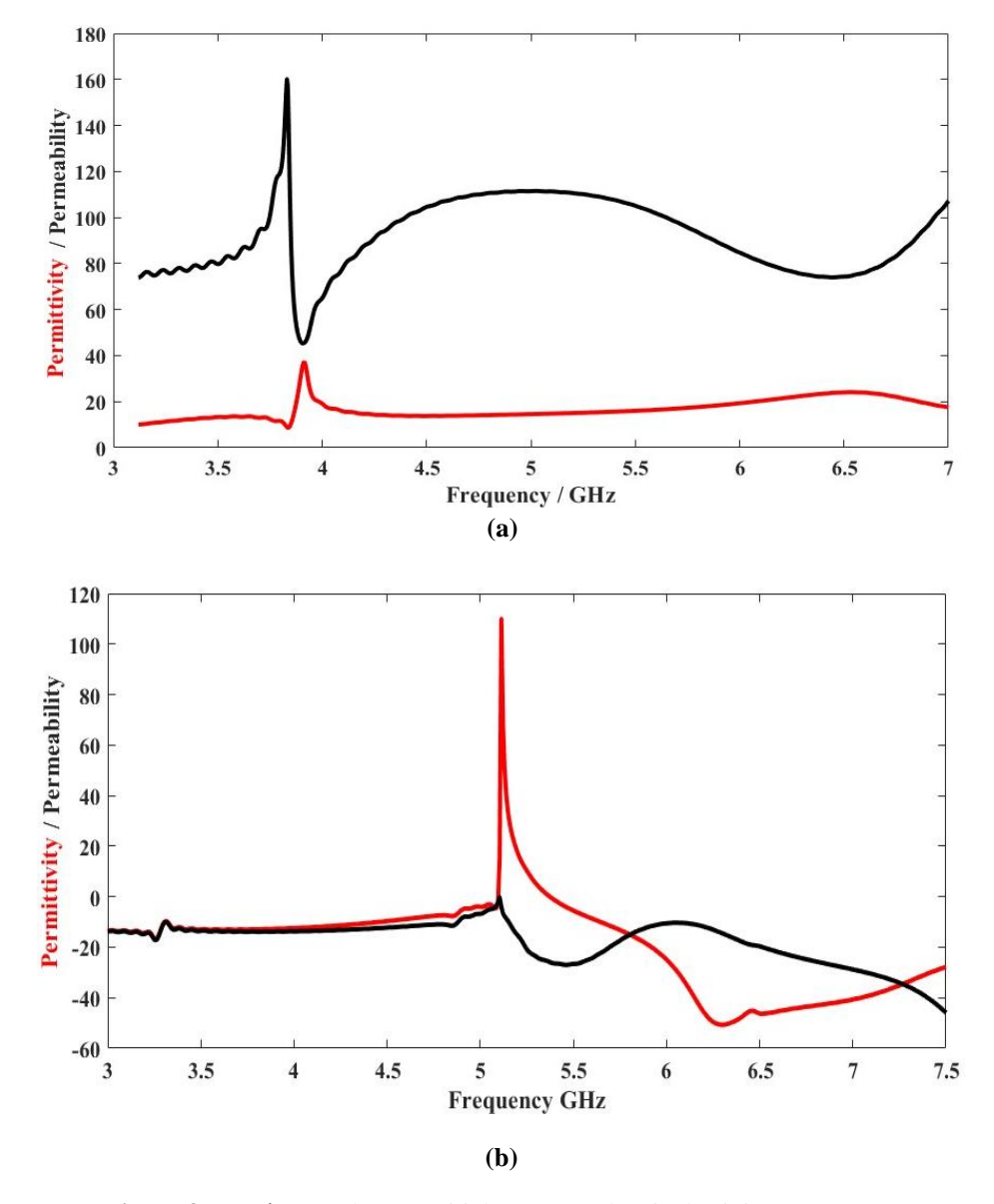
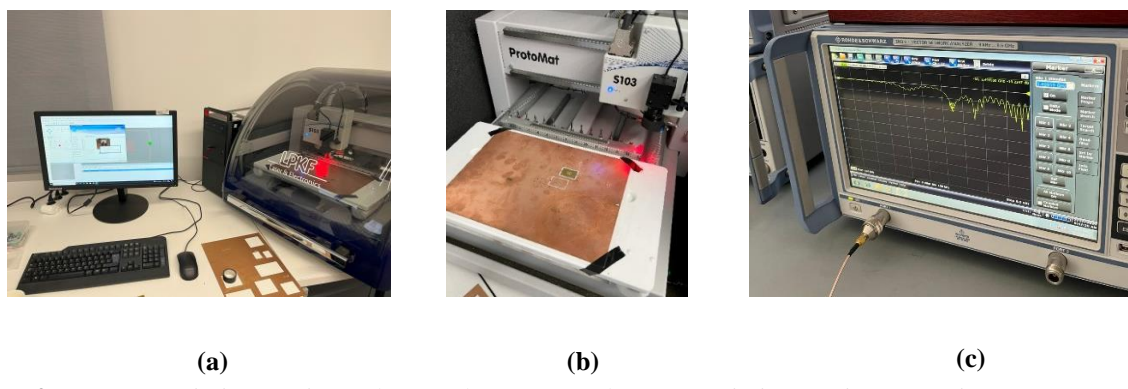


Figure 8.  $\mu$  and  $\epsilon$  Results, (a) Initial Antenna, (b) Final Miniature Antenna

## Antenna fabrication

The final antenna was fabricated via the LPKF Circuit Pro device in (Figure 9.a). The images of the fabricated aperture-coupled microstrip patch antenna are presented in (Figure 10). Reflection coefficients ( $S_{11}$ ) of the fabricated antenna were measured with Rohde & Schwarz ZNB8 Vector Network Analyzer (Figure 9.c).



**Figure 9.** (a) LPKF Printing Device and Control Computer, (b) LPKF Printing Device Engraving Area, (c) ZNB8 Vector Network Analyzer

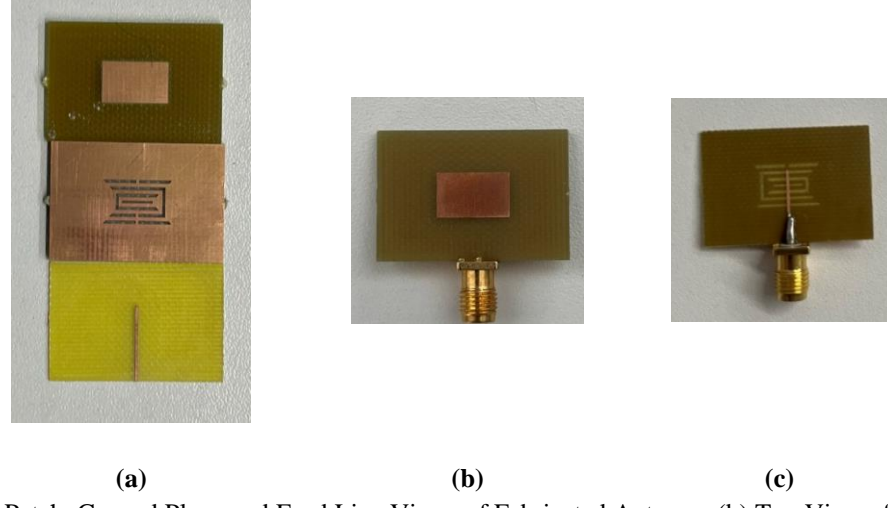


**Figure 10.** (a) The Patch, Ground Plane and Feed Line Views of Fabricated Antenna, (b) Top View of the Final Antenna (c) Bottom view of the Final Antenna

In order to compare the size of the fabricated antenna with a 1U CubeSat, a 1U (10x10x10cm) CubeSat prototype was printed from a 3D printer. The area covered by the fabricated antenna on the CubeSat is clearly seen in (Figure 11).

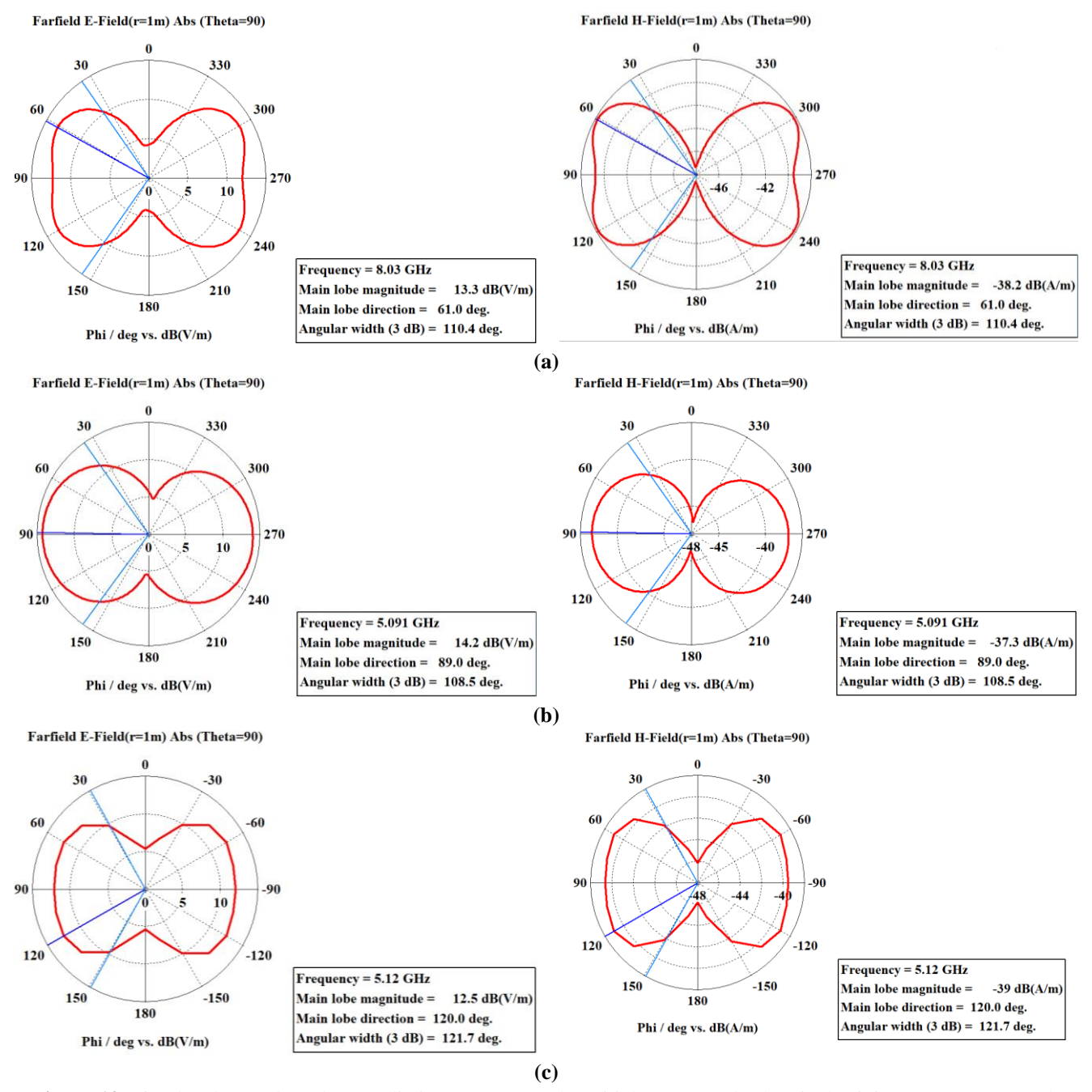


Figure 11. Antenna Size Comparison with 1U CubeSat Size

### RESULTS AND DISCUSSION

### **Simulation Results**

The various analyses were carried out in CST to understand the effects of DGS and the performance of the final miniature antenna design. Fig. 12 depicts the 2-D far-field radiation patterns in the H- and E-planes of the initial antenna, the final miniature antenna, and the conventional antenna, respectively. The radiation pattern of these antennas at the resonance frequencies has been presented for  $\theta = 90$  degrees (xy-plane). The radiation patterns in the xy-plane are dipole type at  $90^{\circ}$ .



**Figure 12.** Simulated E- and H-Plane Radiation Pattern, (a) the Initial Antenna, (b) the Final Miniature Antenna, (c) the Conventional Aperture-Coupled Antenna

The 3D far-field radiation patterns ( $\Phi$ =0) in the simulation environment of the proposed miniature antenna and the conventional antenna are shown in (Figure 13). It is seen that the realized

gain value for the miniature antenna is 4.88 dBi at 5.09 GHz, and the conventional antenna has 6.78 dBi at 5.12 GHz.

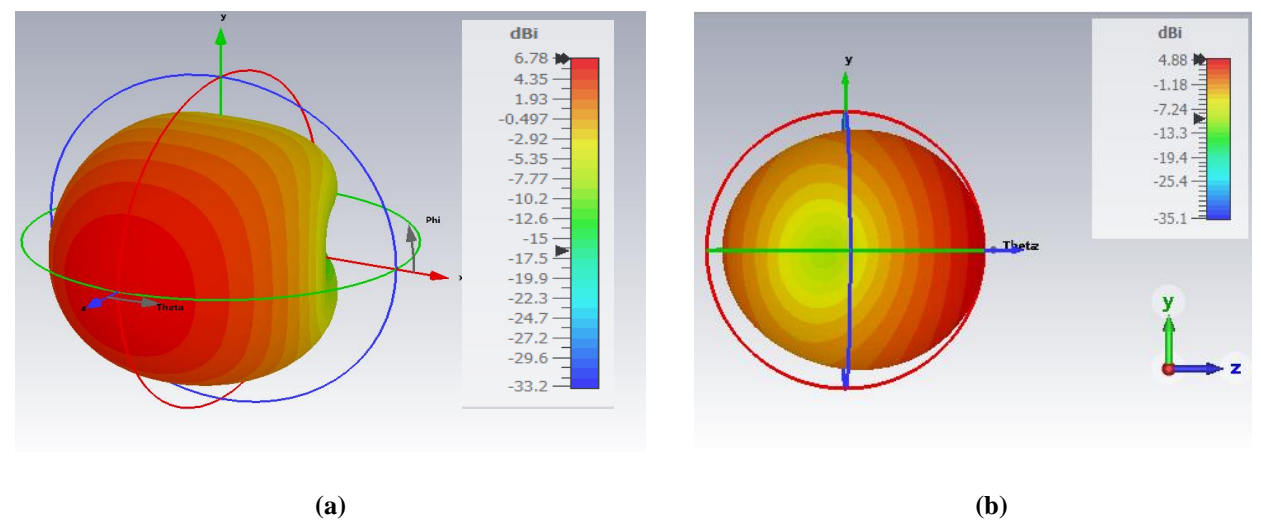


Figure 13. 3D Far Field Radiation Pattern Results (a) the Conventional Antenna, (b) the Final Miniature Antenna

Thus, a high efficiency antenna is obtained by radiating most of the power transmitted to the antenna. The total efficiency analyzed for the miniature antenna, taking into account the losses, is 96%. The surface currents on the designed initial antenna and the final miniature antenna are depicted in (Figure 14). When the surface current distributions are examined, the current flow on the initial antenna (Figure 14.a) is stronger and more continuous than the current flow of the miniature antenna (Figure 14.b) and is also concentrated at the side of the aperture and feed zones. Besides that, it is observed that the surface currents on the metasurface-inspired DGS (Figure 14.b) have a weaker current flow and longer path. The longer path allows the antenna to radiate at a lower frequency.

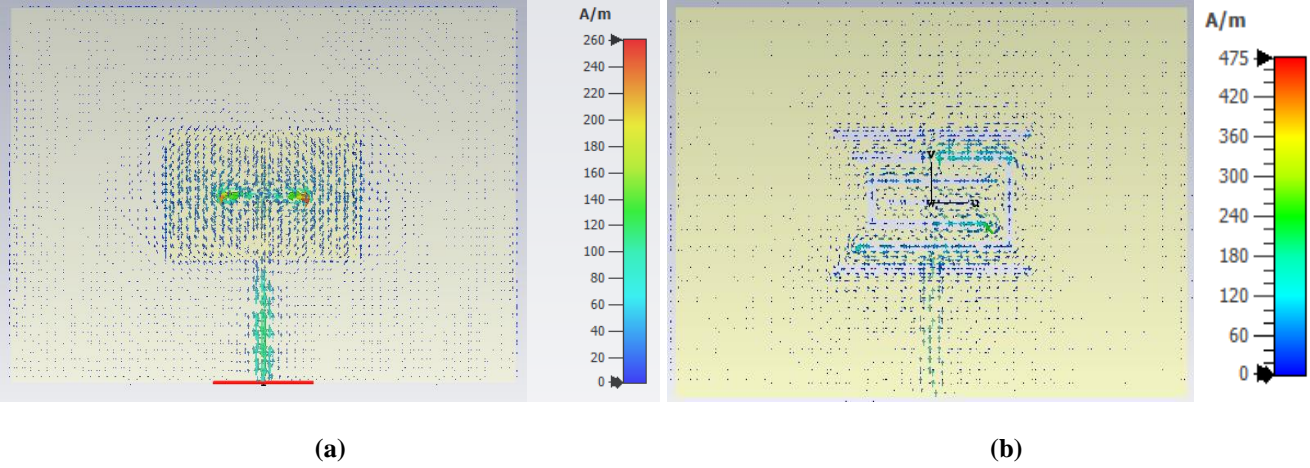


Figure 14. Comparision of Surface Current Distributions, (a) Initial antenna, (b) Final Miniature Antenna

## **Experimental results**

The simulation and measurement results of the reflection coefficients graph of the miniature antenna are depicted comparatively in (Figure 15). As a result of the measurement, it was observed that the fabricated antenna had a -19.3 dB reflection coefficient value at 5.49 GHz frequency. There is a 0.4 GHz frequency shift between the simulation and measurement.

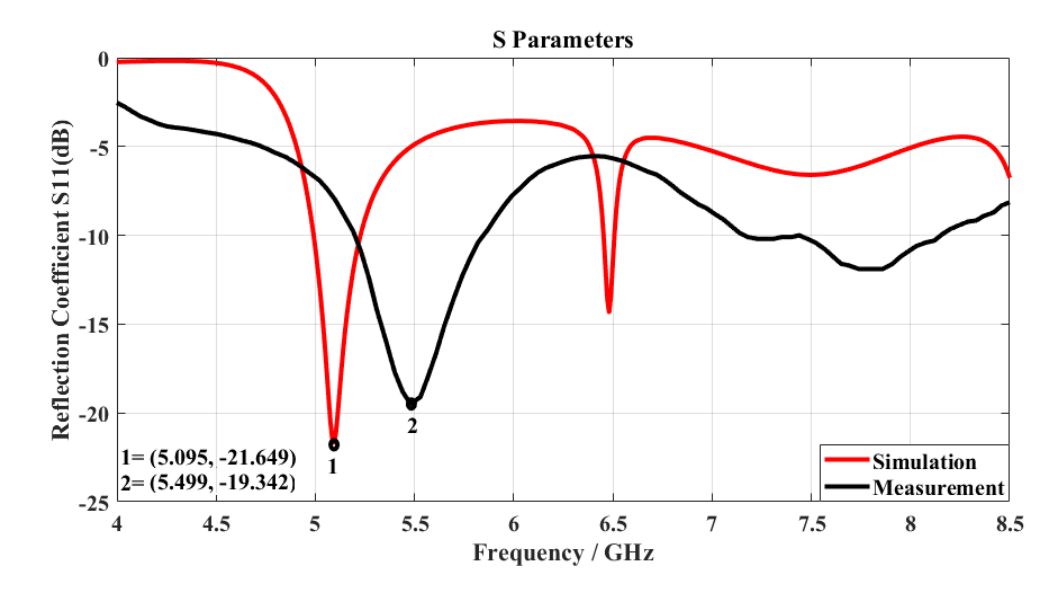


Figure 15. Comparision of Reflection Coefficients Graphs of Simulation and Measurent Results

The reasons for the frequency shift can be listed as follows: The structure is a double-layer, and according to the design in the simulation program, the two layers are completely adhered, but in the fabricated antenna, a gap inevitably forms between the two layers. Positioning, soldering, and aligning the layers of the SMA connector require considerable effort. Moreover, since it is not a fully anechoic chamber, environmental noise affects the antenna parameters. The thickness of the substrate material used is not exactly the same as the antenna in the simulation environment.

**Table 3.** Comparison of the Proposed Miniature Antenna with the Literature

Parameters References	Size of Substrate (mm³)		Size of Patch (mm²)	f <sub>r</sub> (GHz)	Gain (dBi)	Efficiency (%)	BW (MHz)	Min. Rate
(Ramzan & Topalli, 2015)	I.*	40.0x40.0x1.63	15.95x15.95	~5.15	7.35	98.6	103	%51
	M.*	28.0x28.0x1.63	8.0x8.0	~5.15	5.72	78	21.2	
(Zhu et al., 2015)	I.	35.0x35.0x1.63	25.0x19.2	4.0	5.2	80	90	%67
	M.	20.0x20.0x1.63	12.0x10.0	4.0	5.1	84	90	
(Varamini et al., 2018)	I.	40.0x40.0x1.6	Minkowski fractal	7.0	5.8	70	240	0/ 20
	M.	40.0x40.0x1.6	Minkowski fractal	2.5	3.5	72	300	%30
(Painam &	I.	23.0x24.0x0.51	273.45	6.22				%69
Bhuma, 2019).	M.	18.34x14.41x0.51	81.69	6.22	4.13	86.72	280	
(Singh &	I.	80.0x80.0x0.787	42.0x42.0	2.406	5.62	92.07	~40	%50
Lohar, 2022)	M.	40.0x40.0x0.787	20.0x20.0	2.415	6.28	94.66	~60	
[Proposed]	I.	40.7x46.4x1.95	11.9x17.62	5.12	6.78	93	160	04.65
	M.	20.6x30.2x1.95	7.10x11.45	5.095	4.88	96	236	%67

<sup>\*</sup> I.= Initial Antenna, M.= Miniaturized Antenna

## **Discussion**

Thanks to metasurface inspired DGS on the ground surface, the operating frequency of the aperture-coupled antenna operating at 8.031 GHz has been reduced to 5.095 GHz. This means a reduction of approximately 36.0% depending on the frequency. In this study, a conventional aperture-coupled antenna operating at 5.12 GHz was also designed and compared with the miniature antenna in

terms of size. The results obtained are presented in "Table 3". While the area of the conventional antenna is 1890 mm<sup>2</sup>, the area of the miniaturized antenna is 622 mm<sup>2</sup>. This corresponds to a reduction of approximately 67%. In terms of gain, the value of the conventional antenna is 30% better, while the bandwidth is greater in the miniaturized antenna. In addition, a comparative summary of the miniature antenna obtained in this study with the simulation results of the antennas miniaturized using metasurface structures and DGS in the literature is presented in "Table 3". When the "Table 3" is examined, the miniaturization ratio (for physical area) of the proposed miniature antenna is better or approximately the same as other studies in the literature, while it exhibits superior performance compared to the literature in terms of efficiency and especially bandwidth. Although there is a 30% decrease in the gain value of the proposed miniature antenna, the obtained value is comparable to the antennas in the literature and is sufficient for applications.

## **CONCLUSION**

Miniaturization of aperture-coupled antennas by inserting metasurface inspired DGS on the ground plane has been proposed in this paper. The proposed miniature antenna is designed for CubeSAT applications. The final dimensions of the proposed antenna operating at 5.1 GHz are 20.6 mm x 30.2 mm x 1.95 mm. The simulation results are very satisfactory in terms of reflection coefficient, radiation pattern, gain, efficiency, and bandwidth. The use of metasurface inspired DGS on the ground plane has the advantages of giving a good miniaturization rate and a wider bandwidth compared to the conventional antenna operated at 5.1 GHz. In addition, the miniature antenna was fabricated, and it was seen that the measurement results of S<sub>11</sub> parameters were compatible with the simulation results. The proposed antenna is promising for CubeSAT applications.

### **Conflict of Interest**

The article authors declare that there is no conflict of interest between them

### **Author's Contributions**

The authors declare that they have contributed equally to the article.

### REFERENCES

- Abulgasem, S., Tubbal, F., Raad, R., Theoharis, P. I., Lu, S., & Iranmanesh, S. (2021). *Antenna designs for CubeSats: A review. IEEE Access*, 9, 45289-45324.
- ARICAN, G. O., & Karahan, M. (2023). A Novel Broadband Filtenna with using SRR and DGS for Wireless Communication Applications. *Gazi University Journal of Science Part C: Design and Technology*, 1-1.
- Ataş, I., Abbasov, T., & Kurt, M. B. (2020). Gain enhancement and miniaturization of dual-band compact patch antenna. *European Journal of Technique (EJT)*, 10(2), 232-241.
- Baş, R., & Kızılay, A. (2022). Asymmetrical Coplanar Vivaldi Antenna Design. *Avrupa Bilim ve Teknoloji Dergisi*, (34), 724-728.
- Balanis, C. A. (2015). Antenna theory: analysis and design. John wiley & sons.
- Benzaghta, M., Er, B., Bilgin, G., Aydın, E., & Kara, A. (2022). A Miniaturized Multi-layer Microstrip Antenna for Linear Wireless Sensor Network Monitoring Systems. *Gazi University Journal of Science*, 35(3), 875-884.
- Civerolo, M. P. (2010). Aperture Coupled Microstrip Antenna Design and Analysis. California Polytechnic State University.

- Celik, F. T., & Karaçuha, K. (2022). A conical-beam dual-band double aperture-coupled stacked elliptical patch antenna design for 5G. *Turkish Journal of Electrical Engineering and Computer Sciences*, 30(6), 2073-2085.
- Fallahpour, M., & Zoughi, R. (2017). Antenna miniaturization techniques: A review of topology-and material-based methods. *IEEE Antennas and Propagation Magazine*, 60(1), 38-50.
- Iqbal, K., & Khan, Q. U. (2022). Review of metasurfaces through unit cell design and numerical extraction of parameters and their applications in antennas. *IEEE Access*, 10, 112368-112391.
- Liu, S., Theoharis, P. I., Raad, R., Tubbal, F., Theoharis, A., Iranmanesh, S., ... & Matekovits, L. (2022). A survey on CubeSat missions and their antenna designs. *Electronics*, 11(13), 2021.
- Moussa, F. Z., Ferouani, S., & Belhadef, Y. (2022). New Design of Metamaterial Miniature Patch Antenna with DGS for 5G Mobile Communications. *Microwave Review*, 28(2).
- Painam, S., & Bhuma, C. (2019). Miniaturizing a microstrip antenna using metamaterials and metasurfaces [antenna applications corner]. *IEEE Antennas and Propagation Magazine*, 61(1), 91-135.
- Pozar, D. M. (1996). A review of aperture coupled microstrip antennas: History, operation, development, and applications. *University of Massachusetts at Amherst*, 1.
- Raghavendra, C., Ammal, M. N., & Madhav, B. T. P. (2023). Metamaterial inspired square gap defected ground structured wideband dielectric resonator antenna for microwave applications. *Heliyon*, 9(2).
- Ramzan, M., & Topalli, K. (2015). A miniaturized patch antenna by using a CSRR loading plane. International Journal of Antennas and Propagation, 2015(1), 495629.
- Singh, J., & Lohar, F. L. (2022, February). Metamaterial-based miniaturized DGS antenna for wireless applications. In *IOP Conference Series: Materials Science and Engineering* (Vol. 1225, No. 1, p. 012035). IOP Publishing.
- Singh, V., Dwivedi, A. K., & Narayanaswamy, N. K. (2024). Metamaterial/metasurface applications in antenna domain. *Opto-Electronics Review*, e151692-e151692.
- Tadesse, A. D., Acharya, O. P., & Sahu, S. (2020). Application of metamaterials for performance enhancement of planar antennas: *A review. International Journal of RF and Microwave Computer-Aided Engineering*, 30(5), e22154.
- Ünal, E., & Doğan, C. (2020). Metamalzeme Yapılarıyla Fraktal Anten Parametrelerinin İyileştirilmesi. *Çukurova Üniversitesi Mühendislik-Mimarlık Fakültesi Dergisi*, 35(1), 67-78.
- Varamini, G., Keshtkar, A., & Naser-Moghadasi, M. (2018). Miniaturization of microstrip loop antenna for wireless applications based on metamaterial metasurface. *AEU-International Journal of Electronics and Communications*, 83, 32-39.
- Zhu, H. L., Cheung, S. W., & Yuk, T. I. (2015). Miniaturization of patch antenna using metasurface. *Microwave and optical technology letters*, 57(9), 2050-2056.